Pergamon

Journal of Structural Geology, Vol. 17, No. 4, pp. 533 to 547, 1995

0191-8141/95 $9.50+ 0.00

0191-8141(94)00068-9

Chemical changes and fluid–rock interaction in faults of crystalline thrust sheets, northwestern Wyoming, U.S.A.

JAMES V. GODDARD* and JAMES P. EVANS†

Department of Geology, Utah State University, Logan, UT 84322-4505, U.S.A.

(*Received* 16 *November* 1993; *accepted in revised form* 17 *May* 1994)

Abstract—We investigate the degree of fluid–rock interaction in two thrust faults which formed at 4–7 km and 10–12 km depth in crystalline thrust sheets in northwestern Wyoming using whole-rock geochemistry. The fault zones consist of undeformed and unaltered protolith which bounds damaged zones with increased fracture, fault and vein density and chemical alteration, and a fault core comprised of zones of gouge, cataclasite and ultracataclasite. Whole-rock geochemical analyses of major, minor and trace elements in 26 samples document the fluid–rock interactions in the fault zones. Fault-related rocks from the shallow East Fork fault exhibit 10–40% depletion of Si, Al, K, Na and Ca as measured against immobile Ti as reference in the damaged zone, 40–60% depletion of Ca and Na, and 0–20% depletion of Si, Al and K in the fault core. Rocks from the deeper level White Rock thrust exhibit 10–30% depletion of these elements in protocataclasites at the edge of the fault core and up to 65% depletion in the cataclasites and ultracataclasites of the fault core. We interpret these results to show that soluble elements were removed from the fault zones by syntectonic fluid flow. Estimated volume losses in the shallow fault range from 0 to 22%, whereas the deeper level fault experienced 50–65% volume loss in the fault core. Silica loss is used to estimate fluid–rock ratios in the fault zones by assuming a range of temperatures and silica solubilities in the faults during deformation. Volumetric F/R ratios range from 10^2–10^4 for both faults, which yield fluid fluxes in the fault zones of 10^{-6}–10^{-9} m s^{-1} using geologic constraints on the life and geometry of the fault. Depletion and volume loss at deep levels was greater due to hotter fluids and finer grain-size generated by mixed brittle-plastic deformation, whereas at shallow levels, cooler temperatures and purely brittle deformation resulted in vein formation and less chemical fluid–rock interaction.

INTRODUCTION

Fluids profoundly affect the evolution of fault zones in the Earth's crust. Fluids penetrate and influence the development of normal faults (Reynolds & Lister 1987, Bruhn *et al.* 1990, Parry & Bruhn 1990, Glazner & Bartley 1991), reverse faults and thrust sheets (Sibson 1981, Engelder 1984, McCaig 1988, Sibson *et al.* 1988, Forster & Evans 1991), strike-slip faults (Sibson 1987, Chester & Logan 1986, Hickman 1991, Chester *et al.* 1993), mylonitic shear zones (Kerrich 1986, O'Hara 1988, Sinha *et al.* 1988, Selverstone *et al.* 1991), and accretionary prisms (Moore 1989). Fault zones may be fluid-flow conduit/barrier systems that vary over time and space during the life of the fault. Potential sources for fluids at shallow to moderate depths in the crust (<10 km) include meteoric, metamorphically derived, connate, basin and hydrothermal fluids (Engelder 1984, Kerrich 1986, Reynolds & Lister 1987, McCaig 1988, Forster & Evans 1991).

Fluid circulation in fault and shear zones affects the distribution of temperature, pressures and composition of fault-related rocks, which in turn influence the dominant deformation mechanisms and fault rheology. Cataclasis, crystal plasticity, solution transport, reaction weakening, thermal pressurization and hydrolytic weakening are affected by the presence of fluids (cf. Engelder 1984, Mitra 1984, Chester & Logan 1986, Sinha *et al.* 1986, Sibson 1987, Janecke & Evans 1988, Losh 1989, O'Hara & Blackburn 1989, Brantley *et al.* 1990, Evans 1990, Glazner & Bartley 1991, Chester *et al.* 1993). Fluids alter mineral assemblages and rates of chemical and mechanical processes during deformation, which may lead to weakening of fault-related rocks and localization of slip in fault zones (Janecke & Evans 1988, Chester *et al.* 1993).

This paper presents the results of an integrated field, microstructural, and geochemical study of the deformation of the East Fork and White Rock thrusts, northwestern Wyoming, U.S.A. Exposures of fault-related rocks that formed at different structural levels, but within the same tectonic setting, allow us to characterize the spatial and temporal distribution of fractures, veins, and faults at micro- to outcrop-scale in the fault zones. We use mineralogic and whole-rock geochemical analyses to estimate the nature and degree of fluid–rock interactions in the fault zones. We estimate the bulk-rock volume losses and fluid fluxes associated with fault-zone fluid flow, and examine how fluid flow may have varied spatially and temporally in the fault zone and at different structural levels. Finally, we integrate these results into a model that characterizes fluid flow through brittle and semi-brittle fault zones at shallow crustal levels.

*Present address: Environmental and Engineering Solutions, Inc., Logan, UT 84322, U.S.A.
†Author to whom all correspondence should be addressed.

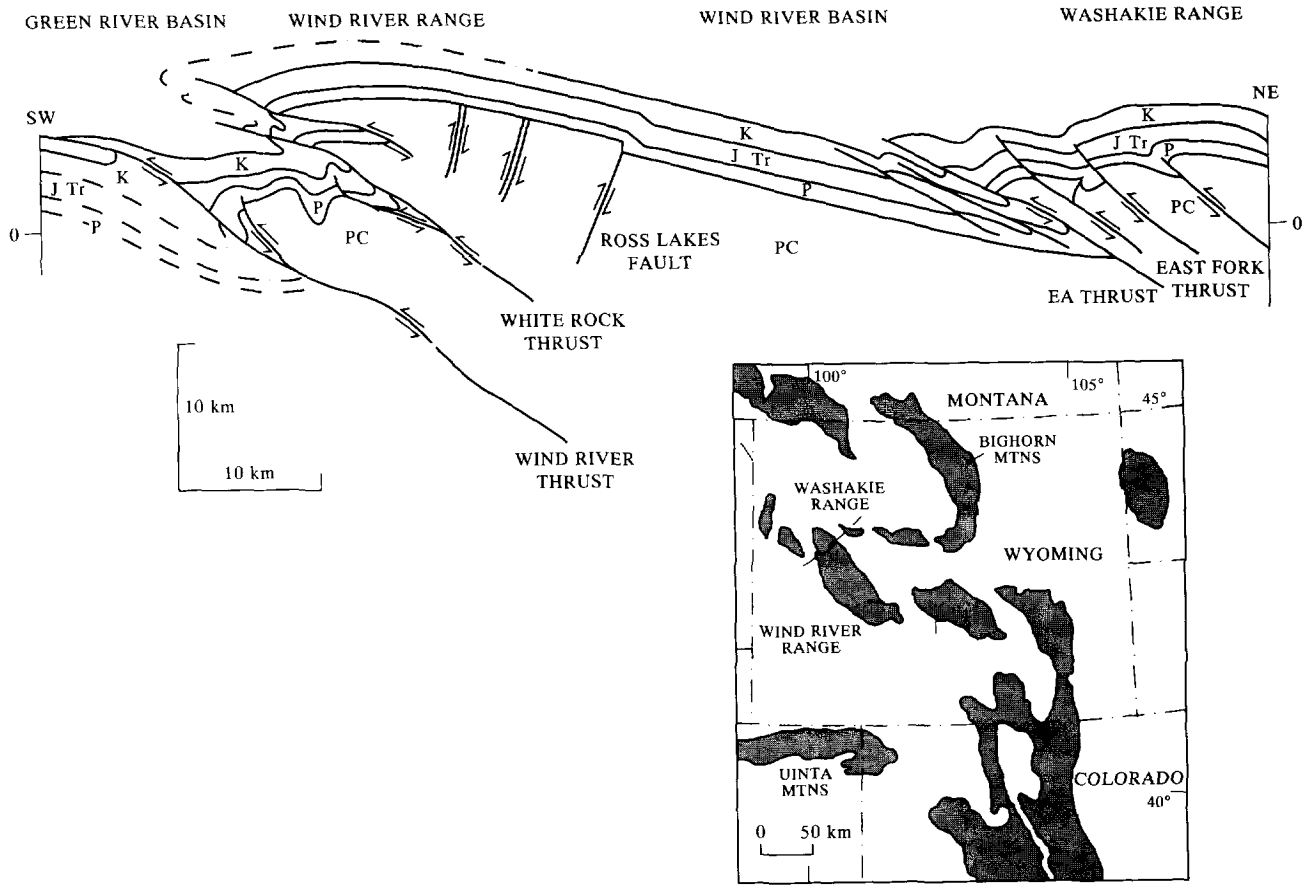

Fig. 1. Down plunge projection towards the north–northwest of the northern part of the Wind River Range and the Washakie Range. Rock units are: PC—Precambrian granite and gneiss; P—Paleozoic sedimentary rocks; J Tr—Jurassic–Triassic sedimentary rocks; K—Cretaceous sedimentary rocks. Down plunge projection is based on Mitra (1984) and Evans (1993), and this study. Solid arrow shows approximate location of White Rock thrust area; open arrow indicates location of the East Fork site. (b) Inset map which shows location of line of section.

Geologic setting

Ideally, we would examine a single fault at different structural levels to characterize fluid–rock interactions in a large fault. However, a single fault zone is rarely exposed over a wide range of structural levels. To infer the structure and fluid–rock interactions at different structural levels, we examined fault-related rocks formed at two structural levels in the White Rock and East Fork thrusts in the Wind River Range and Washakie Ranges, respectively (Fig. 1). The White Rock thrust is an imbricate to the Wind River thrust (Richmond 1945, Mitra & Frost 1981, Mitra 1984, Mitra *et al.* 1988) and represents the deepest structural level discussed in this paper. Displacement on the White Rock thrust is about 8 km, and the fault places Precambrian granitic gneisses on overturned Paleozoic and Mesozoic sedimentary rocks (Fig. 1). Restored cross-sections suggest that the part of the White Rock fault we examined deformed at 10–12 km depth, and overburden thickness of 10–12 km existed at the time of initial thrusting (Mitra 1984). Evidence for fluid infiltration into this fault zone includes laumontite and chlorite veins, and syntectonic alteration of feldspars to phyllosilicates in the core of the fault.

The East Fork faults are hanging wall imbricates of the EA thrusts (Evans 1993), which juxtapose Precambrian granite and gneiss over Paleozoic and Mesozoic sedimentary rocks of the Wind River basin. Fault zones in the East Fork area formed at a depth of 4–7 km, have granite and gneiss in both the footwall and hanging wall, and have 2–4 km of slip (Evans 1993). Quartz veins, iron-oxide-filled fractures, and syntectonically altered feldspars indicate fluids infiltrated the fault during slip (Evans 1990).

The faults we examined are relatively simple structures with well-defined histories and contain abundant evidence for syntectonic fluid flow. Fluid flow was probably topographically driven (Forster & Evans 1991), and the topography was developed during thrust sheet development (Evans 1993). Fluid sources in this setting include meteoric water, formation waters trapped in the crystalline rocks, and fluids in the sedimentary rocks under the thrust sheets. We first describe the outcrop and microstructural character of the faults and the results of our geochemical analyses. We use the

results of this work to determine rock volume losses in the fault zones, and finally we integrate the results into a model for the hydrologic character of the faults.

MESOSCOPIC AND MICROSCOPIC DESCRIPTIONS OF THE FAULTS

We briefly summarize the structure and microstructures of the faults that are relevant to the fluid flow history of the faults. Details regarding fault zone microstructures and deformation mechanisms can be found in Evans (1988, 1990, 1993), Mitra (1984, 1990), Mitra *et al.* (1988), and Yonkee & Mitra (1993).

East Fork fault

Faults which comprise the East Fork fault zone are narrow faults or wide zones of gouge. Narrow faults consist of well-foliated, indurated, silica-cemented, fine-grained gouge and cataclasite, both of which consist of fine-grained gouge and cataclasite, with crude to well-defined foliation. The wide gouge zones are up to 6 m wide and separate lozenges of fractured and altered protolith (Evans 1993). The wide faults, and the entire fault zone, are internally zoned. These zones are: (1) unaltered protolith, (2) fractured and faulted damaged zone, and (3) gouge and cataclasite zones. Brittle deformation and comminution of feldspars and quartz were the dominant deformation mechanisms in the faults (Evans 1988, 1990). Syntectonic alteration of feldspars to clays resulted in development of foliated cataclasites.

White Rock fault

The White Rock thrust is a ~ 50–70 m thick fault zone between Archean granodiorite gneiss and Mississippian Madison Limestone (Fig. 2a)(Mitra 1990, Yonkee & Mitra, 1993). The fault strikes N–NW and dips 20°–70°NE, and movement along the fault was principally dip-slip. The White Rock thrust is zoned into: (1) relatively undeformed and unaltered protolith (Fig. 2a), (2) fractured, veined, and faulted damaged zone (Figs. 2b & c), and (3) crude to well-foliated gouge, protocataclasite, cataclasite and ultracataclasite (the fault core) (Fig. 2d). The unaltered protolith is granitic–granodiorite, and consists of microcline (~35%), plagioclase (~30%), quartz (~27%), and biotite/chlorite (~5%) with accessory rutile, hematite, ilmenite and other opaque Fe–Ti oxides (~3%). The fractured damaged zone is 1–40 m thick, and contains small-displacement faults, fractures, and veins in the damaged zone which are subparallel to the main fault (Fig. 2c).

The core of the fault zone consists of a narrow zone of intense deformation of non-foliated to foliated ultracataclasites 0.5–10 m thick which surround lenses of less deformed, veined, non-foliated to foliated cataclasites and protocataclasites. Microscopic foliation in the ultracataclasite is defined by syntectonic alignment of iron oxides, clay and mica minerals. The contact between damaged zone and the fault core is sharp (Fig. 2d), or consists of a zone 1–10 cm thick of cataclasites or ultracataclasites indicating localized slip at the edge of the fault zone. The cataclasites and ultracataclasites in the core of the White Rock thrust exhibit concentrated cataclasis, fluid–rock chemical reaction, and solute transport and deposition (Mitra 1984, 1990, Yonkee & Mitra 1993). The protocataclasite and cataclasite matrix is made up of comminuted quartz and feldspar (microcline and plagioclase), fine-grained micas (mostly biotite and chlorite), kaolinite, laumontite and minor iron oxides and opaque minerals (Fig. 3a). Larger clasts of feldspar, quartz, and opaque minerals make up the framework.

The ultracataclasite matrix is made up of biotite, montmorillonite, laumontite, kaolinite, and minor iron oxides, quartz, and feldspars (Fig. 3b). The ultracataclasites are composed of ~1–10% grains resolvable by petrographic scope, and ~90–99% matrix. Optically resolvable material consists of ~30% microcline, ~30% opaques (Ti-bearing minerals), ~25% quartz, and ~15% plagioclase. A similar distribution exists in the cataclasite, suggesting that opaque minerals and microcline are the most stable minerals in the fault with quartz and plagioclase more susceptible to dissolution and chemical reactions. The Ti- and Fe-bearing minerals remained relatively chemically immobile throughout deformation.

Throughout most of the White Rock thrust's history, the fault core was bounded on both sides by Precambrian granitic protolith. Of the 10–12 km of displacement, only about 2 km of displacement occurred with sedimentary rocks in the footwall. Thus, we assume a granitic protolith mineralogy dominated during deformation and subsequent alteration of the fault, and that the underlying Paleozoic sedimentary rocks affected the fault very late in its history. The presence of laumontite in damaged zone veins and the fault core indicate that most of the fluids responsible for fault-related mineralization were in the fault zone before the Archean rocks were thrust over the carbonate-rich Paleozoic sedimentary rocks. Laumontite is stable under extremely low pCO_2 conditions (Zen 1961, Thompson 1971, W. T. Parry personal communication 1993), and is stable in the presence of calcite only under very special conditions (Thompson 1971). Thus it is unlikely that laumontite veins developed by flow of CO_2 rich fluids from the Paleozoic carbonates.

Numerous intricate networks of outcrop- to thin section-scale, folded and faulted laumontite veins in both the damaged zone and fault core suggest syntectonic, hydrothermal alteration played an important role in deformation. Within the core and the damaged zone, cross-cutting sets of fractures, faults, veins, and foliations imply repeated episodes of fluid-assisted deformation (Figs. 3c–e).

GEOCHEMISTRY OF FAULT ZONE ROCKS

We use X-ray diffraction and X-ray fluorescence spectrometry to characterize the composition of the fault zone rocks. Major-, minor-, and trace-element geochemical analyses of fault-related rocks reveal relative concentrations of immobile and mobile constituents within the fault zone, which enable us to calculate volume loss and fluid–rock ratios in the fault zone (Gresens 1967, Grant 1986, O'Hara 1988, O'Hara & Blackburn 1989, Sinha *et al.* 1988). Whole-rock geochemical analyses were performed by X-Ray Assay Laboratories (XRAL) in Don Mills, Ontario, Canada. Eleven samples from the East Fork fault and 15 samples from the White Rock thrust were analyzed (Table 1).

The open system behavior of most fault zones with respect to fluids requires that a reference frame be established for discussing whole rock geochemical data. Based on our microstructural observations and the work of others, we use Ti (as TiO_2) as the immobile constituent within the fault zones. Geochemical studies of metasomatized rocks and shear zones support the immobility of Ti as well as Mg, Mn, Zr, Y and P (Correns 1978, Dostal *et al.* 1980, Hanson 1980, Floyd & Winchester 1983, Winchester & Max 1984, Sinha *et al.* 1986, Vocke *et al.* 1987, O'Hara 1988, O'Hara & Blackburn 1989, Glazner & Bartley 1991, Selverstone *et al.* 1991). We interpret the enrichment of Ti and associated high-field strength cations as due to losses of soluble elements, and we estimate the relative amount of volume loss and fluid–rock interaction by examining the changes in element abundances relative to the immobile element(s). To prevent a single analysis from skewing the results, we examined where ever possible variations of mean values of each calculated oxide from averaged analyses of protolith, damaged zone rock, cataclasite and ultracataclasite samples. Protolith samples discussed here were collected 50–200 m from the fault core and damaged zone samples from 50 to 1 m from the core. Protocataclasites, cataclasites, and ultracataclasites come from the fault core.

Traverses across the East Fork fault zone indicate moderate losses in SiO_2, Al_2O_3, CaO, Na_2O and K_2O and moderate gains of Fe_2O_3, MgO and LOI (lost on ignition, probably H_2O and CO_2) in the damaged zone (Fig. 4a). In contrast, the gouge/cataclasite zone indicates little loss of SiO_2, MgO and K_2O, accompanied by losses in Na_2O and CaO. Fe_2O_3 and LOI remains mostly unchanged from the damaged zone.

Losses of SiO_2, Al_2O_3 and alkalis in the damaged zone are due to hydrolysis of feldspars into sericite, clays, and other phyllosilicates and to the transport of soluble elements out of the fault zone. Many damaged zone macro- and microscopic fractures are filled and lined with kaolinite and Fe–Mg oxides, explaining the gains in Fe_2O_3 and MgO in the damaged zone.

With the exception of SiO_2, K_2O and P_2O_5, other oxides follow the same trends in the gouge/cataclasite zone as the damaged zone of the East Fork fault zone. Two models may explain the geochemical signature of the gouge zone of the East Fork faults. The first model consists of an early-stage damaged zone from which fault gouge developed, resulting in decreased permeability and fluid flux. During subsequent slip, the damaged zone would have maintained some permeability, and rock in the damaged zone continued to react with fluids; fluids in the fault core may have become saturated with respect to silica and Fe_2O_3, resulting in precipitation in the fault core. More fluid could not penetrate the fault core due to low permeabilities in the fault core (Forster *et al.* 1994). This could explain the increase in SiO_2 in the gouge/cataclasite zone relative to the damaged zone.

A second model suggests that little chemical fluid–rock interaction occurred in the early stages of faulting whereas later stages of thrust sheet development resulted in greater chemical activity. Either the thrust at this level received more fluid as thrusting continued, or fluids with greater chemical activity from depth flowed along this part of the fault in its more mature stage.

Chemical variations across the much larger displacement White Rock thrust indicate dramatic losses of SiO_2, Al_2O_3, CaO and Na_2O from protolith to ultracataclasite (Fig. 4b). As much as 75% of these elements are lost, whereas MnO, Fe_2O_3, P_2O_5, TiO_2 and MgO are either unchanged or gain slightly from the protolith to ultracataclasite. Conversely, K_2O increases by about 90% in the protocataclasite zone, and it drops and follows the trend of the other alkalies in the cataclasite zone. LOI steadily increases towards the ultracataclasites.

These results indicate that feldspar alteration and quartz dissolution reactions may have progressed further to completion in the White Rock thrust, and Si and Na were released in large quantities with other mobile species from the cataclasites and ultracataclasites. The changes in Ca and Al content, and the presence of laumontite veins, indicates at least local transport of Ca and Al. Few quartz veins are observed in outcrop or thin section, indicating that silica was transported at least as far as the several hundreds of meters of available exposure. The behavior of K_2O may be explained by slightly more stable behavior of microcline, which is not as altered in the damaged zone as is plagioclase. Increased slip and grain-size reduction in the fault core may have accelerated microcline alteration and released K in the fault core. Immobile elements in the fault core include Ti, Mn, P and to a lesser extent, Mg and Fe, and were concentrated in the fault zone.

The large losses of silica and alkalis are consistent with the breakdown of feldspars and the release of these components in a fluid. Based on petrographic observations, chemical reactions leading to the breakdown and alteration to kaolinite, montmorillonite, and laumontite in the faults include:

$$\underset{\text{quartz}}{SiO_2} + H_2O \leftrightarrow \underset{\text{dissolved silica}}{H_4SiO_4} \quad (1)$$

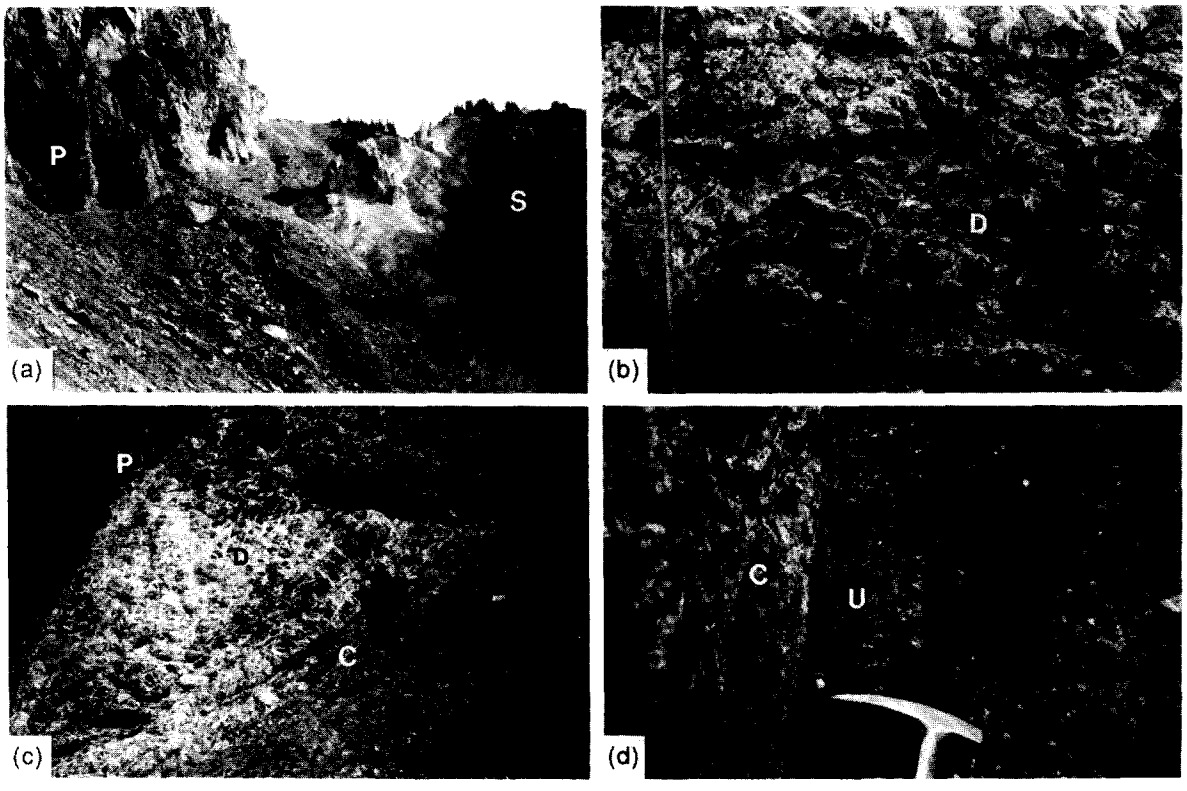

Fig. 2. Field views of the fault zones. (a) View southward of White Rock fault zone (F). Zone is ~50 m wide and is bounded by protolith granite (P) in the hanging wall and Paleozoic sedimentary rocks (S) in the footwall. (b) Granitic protolith (P) in sharp fault-contact (arrows) with veined, faulted, and fractured protocataclasite in the damaged zone (D). The protolith (P) and damaged zone (D) contact (arrows) is characterized by a thin (~1–10 cm) zone of cataclasite and ultracataclasite. Field of view is 1 m high. (c) Intricate network of white laumontite veins in the damaged zone (D) adjacent to protolith granite (P) and the fault core (C). View is oblique to fault strike. Person is standing in the damaged zone, which contains fault-parallel fractures and faults oriented in the direction of the arrows. (d) Intensely veined and faulted cataclasite (C) developed in granitic protolith, in sharp fault contact with ultracataclasite (U).

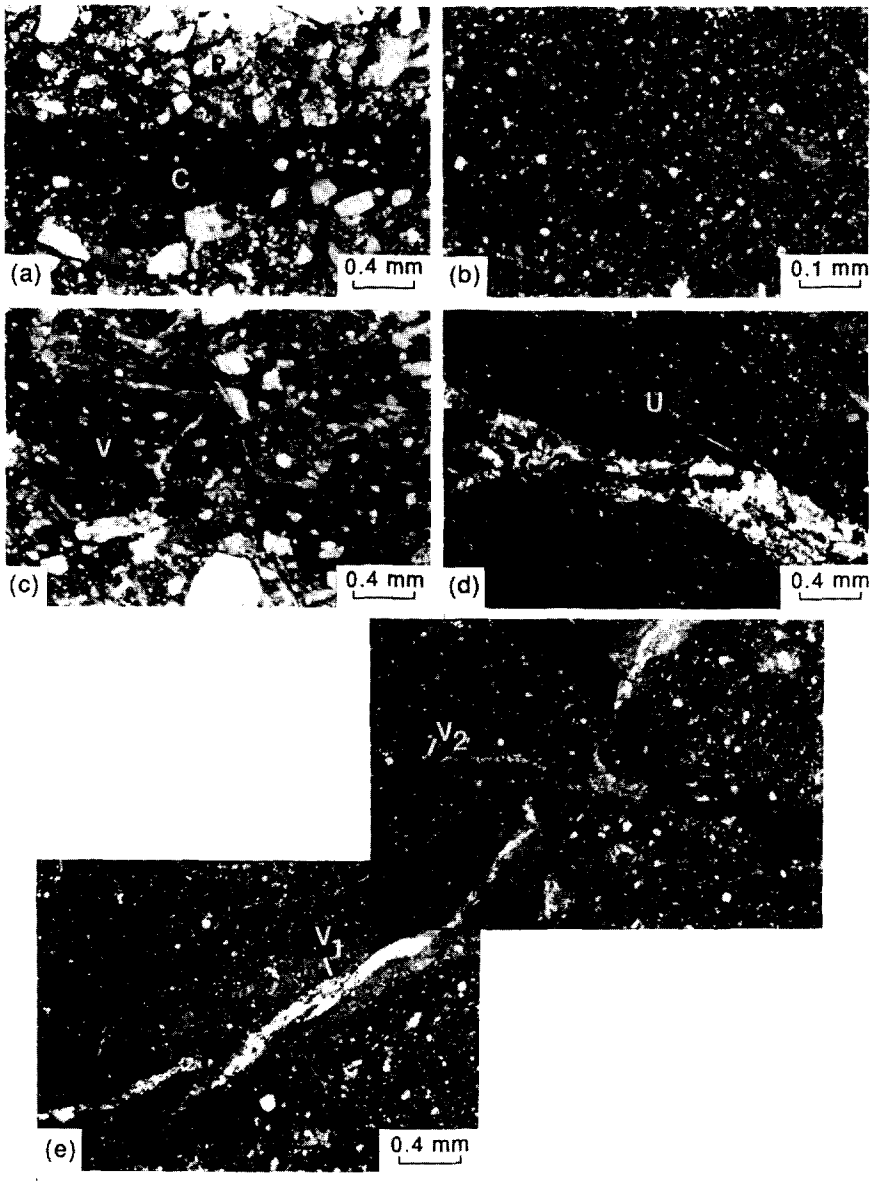

Fig. 3. Microstructures of fault related rocks from the White Rock thrust. (a) Deformation is localized in protocataclasites (P), which consists of zones of cataclasite (C) in which slip becomes focused and comminution is concentrated. Angular quartz and feldspar grains lie in a matrix of clays and iron oxides. Plane polarized light photomicrograph. (b) Fault core rocks consist of ultracataclasites composed of very fine-grained quartz in a matrix of highly comminuted clay, feldspars, and zeolites. Cross-polarized light photomicrograph. (c) Laumonite–hematite vein fragment (V) lies in a matrix of ultracataclasite and is offset by small faults. Clast indicates previous episode of fluid flow and subsequent deformation. Plane-polarized light photomicrograph. (d) Wispy, euhedral laumonite grains in veins cutting the ultracataclasite (U). Cross-polarized light photomicrograph. (e) Episodes of fluid flow are suggested by cross-cutting veins V_1, cut by V_2, in the fault core, parallel to ultracataclasite. Cross-polarized light photomicrograph.

Table 1. Whole rock X-ray flourescence analyses of the East Fork thrust granites and associated fault rocks. Error is ± 0.01% wt. for major and minor element analyses; ± 10 ppm for trace elements

	Protolith	Damaged zone			
Sample	EFP-YR	EF2A-dam	EF2-dam	EF4A-dam	EFJE4-dam
SiO_2(wt%)	72.7	73.3	70.9	74.3	71.1
TiO_2	0.164	0.231	0.224	0.234	0.166
Al_2O_3	14.1	13.2	13.0	13.1	13.7
Fe_2O_3	1.14	1.29	1.73	1.61	3.20
MnO	0.01	0.01	0.03	0.02	0.03
MgO	0.28	0.20	0.78	0.44	0.28
CaO	1.47	0.63	1.70	0.70	1.68
Na_2O	3.51	3.54	2.92	3.17	3.31
K_2O	3.93	4.91	4.58	4.50	3.87
P_2O_5	0.05	0.05	0.03	0.03	0.04
LOI	1.45	1.20	3.70	1.62	1.75
Total	99.0	98.8	99.9	100.0	99.3
Rb(ppm)	90	107	100	104	96
Sr	230	146	233	226	258
Y	<10	<10	<10	<10	27
Zr	155	164	189	199	226
Cr	<10	<10	57	54	<10
Nb	21	19	25	<10	19
Ba	1590	1690	1640	1650	1120

	Vein	Damaged/gouge		Gouge/cataclasite		
Sample	EF2-vein	EF2-88	EF14a-88	EF2c-91	EFJE-2	EF4B
SiO_2(wt%)	96.6	79.0	77.4	78.6	75.3	75.6
TiO_2	0.018	0.115	0.186	0.156	0.190	0.179
Al_2O_3	1.50	10.7	12.1	10.2	12.4	12.4
Fe_2O_3	0.03	0.65	1.36	1.30	1.96	1.17
MnO	0.01	0.01	0.02	0.01	0.01	0.01
MgO	0.08	0.21	0.44	0.20	0.45	0.14
CaO	0.21	0.39	0.76	0.40	0.51	0.27
Na_2O	0.28	1.19	3.61	2.13	0.82	2.75
K_2O	0.71	5.59	0.34	4.01	3.66	4.82
P_2O_5	0.02	0.03	0.04	0.05	0.05	0.05
LOI	0.47	1.15	3.80	1.35	3.50	1.39
Total	100.0	99.3	100.1	98.6	99.0	99.0
Rb(ppm)	31	163	31	91	106	89
Sr	<10	79	125	83	200	107
Y	<10	<10	<10	10	13	<10
Zr	<10	59	111	116	133	144
Cr	<10	<10	18	<10	<10	<10
Nb	19	28	24	<10	20	15
Ba	432	1700	159	1380	1210	1650

	Protolith		Protocataclasite					Vein	
Sample	WR7-91	WRe-92	WR6-91	WR13-91	WR8a-91	WR5-91	WR16-91	WR4-91	WR19-91
SiO_2(wt%)	68.5	70.3	63.2	65.2	66.9	67.7	65.3	54.3	56.6
TiO_2	0.366	0.274	0.162	0.529	0.112	0.174	0.334	0.172	0.225
Al_2O_3	16.2	14.5	16.7	15.6	15.8	14.5	15.4	19.2	19.0
Fe_2O_3	3.59	1.72	3.08	3.13	1.66	1.41	2.58	1.52	1.79
MnO	0.03	0.02	0.02	0.04	0.01	0.01	0.03	0.03	0.02
MgO	0.70	0.66	0.24	1.78	0.22	0.44	0.97	0.75	0.91
CaO	4.22	1.44	1.05	2.42	0.91	1.89	2.57	8.98	8.02
Na_2O	4.65	3.36	1.97	3.23	2.02	1.90	2.75	1.86	0.95
K_2O	1.36	5.64	10.3	5.17	9.12	6.98	4.99	1.74	2.57
P_2O_5	0.18	0.12	0.21	0.17	0.11	0.07	0.13	0.07	0.08
LOI	0.77	1.30	0.77	1.55	0.90	3.70	3.50	10.9	10.0
Total	100.4	99.7	98.4	99.2	98.3	99.2	98.9	99.6	100.3
Rb(ppm)	50	99	149	96	142	132	96	32	59
Sr	462	396	476	417	403	362	297	280	286
Y	16	19	38	15	<10	<10	<10	<10	<10
Zr	194	130	29	59	12	82	214	19	119
Cr	24	<10	<10	12	<10	<10	<10	<10	12
Nb	16	14	15	21	29	31	22	13	15
Ba	461	2770	5660	2710	4540	3360	2280	392	634

Table 1. *Continued*

	Cataclasites				Ultracat.	Protocat.
Sample	WR15-91	WR10-91	WR8b-91	WR14b-91	WRf-92	WR1-91
SiO_2(wt%)	59.3	58.3	59.1	58.6	57.6	67.6
TiO_2	0.746	0.529	0.433	0.602	0.728	0.283
Al_2O_3	16.3	16.2	16.3	15.1	14.9	14.5
Fe_2O_3	6.64	4.80	4.80	5.56	5.40	2.41
MnO	0.08	0.06	0.05	0.05	0.05	0.02
MgO	2.34	1.77	1.42	2.12	2.49	0.66
CaO	6.37	3.91	2.76	4.45	4.65	1.24
Na_2O	4.29	1.95	2.00	1.97	2.38	2.20
K_2O	1.58	5.19	6.93	3.07	3.01	7.29
P_2O_5	0.29	0.31	0.33	0.28	0.30	0.10
LOI	2.45	5.08	3.70	7.95	8.05	1.75
Total	100.6	98.5	98.3	100.0	99.8	98.3
Rb(ppm)	31	103	126	81	76	168
Sr	1130	351	370	599	425	170
Y	63	39	36	38	53	<10
Zr	233	136	119	179	224	245
Cr	47	51	17	24	54	<10
Nb	19	<10	25	34	28	19
Ba	429	2410	3340	1200	1430	1320

$$2\underset{\text{albite}}{NaAlSi_3O_8} + 9H_2O + 2H^+ \leftrightarrow \underset{\text{kaolinite}}{Al_4Si_4O_{10}(OH)_8} + 2Na^+ + \underset{\text{dissolved silica}}{8H_4SiO_4} \quad (2)$$

$$42\underset{\text{albite}}{NaAlSi_3O_8} + Ca^{2+} + 4H_2O \leftrightarrow \underset{\text{laumontite}}{CaAl_2Si_4O_{12}\cdot 4H_2O} + 2Na^+ + \underset{\text{amorphous}}{2SiO_2} \quad (3)$$

$$5\underset{\text{anorthite}}{CaAl_2Si_2O_8} + \underset{\text{dissolved silica}}{2H_4SiO_4} \leftrightarrow \underset{\text{laumontite}}{CaAl_2Si_4O_{12}\cdot 4H_2O} \quad (4)$$

$$2\underset{\text{microcline}}{KAlSi_3O_8} + 2H^+ + 9H_2O \leftrightarrow \underset{\text{kaolinite}}{Al_2Si_2O_5(OH)_4} + \underset{\text{dissolved silica}}{4H_4SiO_4} \quad (5)$$

$$47\underset{\text{kaolinite}}{Al_2Si_2O_5(OH)_4} + 8SiO_2 + 2K^+ \leftrightarrow 6[(Al_2)(Si_{3.67}, Al_{0.33})O_{10}(OH)_2]\underset{\text{K-montmorillonite}}{K_{0.33}} + 7H_2O + 2H^+. \quad (6)$$

Most of these reactions require water or H^+ ions, and the reactions typically liberate relatively large amounts of silica into solution (Garrels & Christ 1965, Faure 1991).

VOLUME LOSS AND FLUID–ROCK RATIOS

Evaluation of volume loss and fluid flux in fault zones requires knowledge of the composition of undeformed and deformed rocks. We use the methods of Gresens (1967) as adapted by Grant (1986), O'Hara (1988) and Goddard (1993) to determine the volume changes within the fault zone.

We use the relationships for volume loss:

$$M_l = [(1/S) - 1] \times 100, \quad (7)$$

$$V_l = [(1/S)(g^{fa}/g^{pr}) - 1] \times 100, \quad (8)$$

where S is the slope of the immobile isocon (e.g. $S \approx (C^{fa}_{Ti}/C^{pr}_{Ti})$), and M_l and V_l are in percent loss or gain of a given element, and g^{fa}/g^{pr} is the ratio for the specific densities of the rock (Grant 1986), to estimate mass and volume loss in the damaged zone that range from 0 to 22%. Using the immobile isocon slope of 1.29 for the East Fork damaged zone (Fig. 5a) fitted to the origin and Ti, Zr, Fe_2O_3 and MgO to calculate the volume factor, and the densities and chemical compositions, the following balanced component equation can be written for the East Fork damaged zone:

100 g protolith granite − 18.6 g SiO_2 − 4.1 g Al_2O_3 − 0.6 g CaO − 1.1 g Na_2O − 0.6 g K_2O → 74.6 g damaged rock + 0.3 g Fe_2O_3 + 0.1 g LOI. (9)

The balanced equation implies only moderate losses in SiO_2 and Al_2O_3 with negligible losses in CaO, Na_2O, and K_2O, and small gains in Fe_2O_3. Components with negligible losses or gains of <0.01 g were not listed in the balanced equation.

For the East Fork gouge/cataclasite zone (Fig. 5b), the constant mass isocon has a slope of one, and the constant volume isocon has a slope of 1.04 ($\rho^{fa}_{gouge}/\rho^{pr}$ = 2.72/2.62). The immobile isocon is best-fit through TiO_2, Zr, Fe_2O_3 and MgO and leads to a slope of 1.04, nearly identical to the constant volume isocon. Mass loss is ~ 3% with no volume loss in the gouge/cataclasite zone. The balanced component equation for the East Fork gouge/cataclasite is:

100 g protolith granite − 2.75 g Al_2O_3 − 1.1 g CaO − 1.7 g Na_2O → 92.0 g gouge/cataclasite + 1.5 g SiO_2

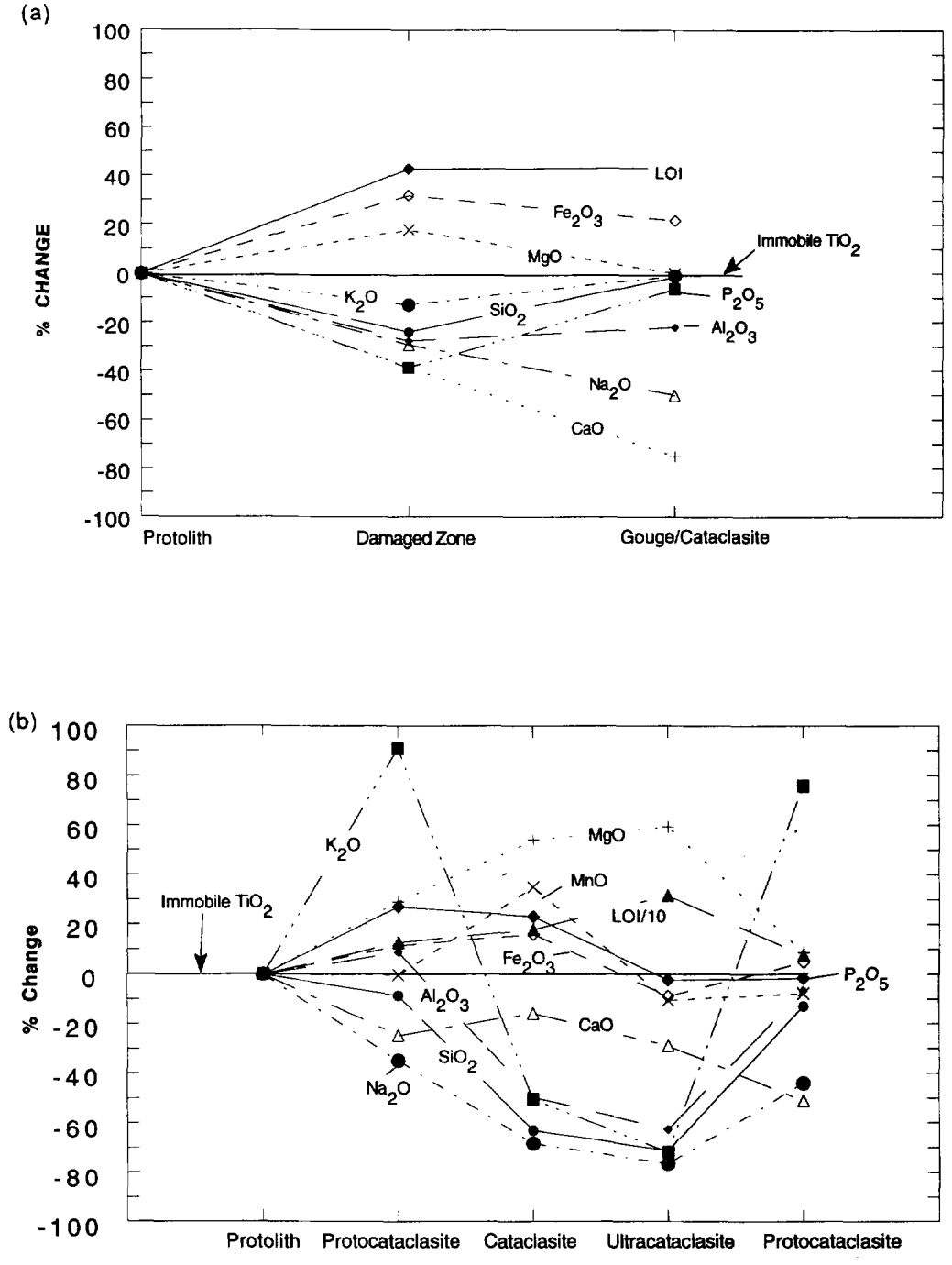

Fig. 4. Changes in major element content in samples from different parts of the fault zone as plotted against immobile TiO_2. (a) Traverse across the East Fork fault shows modest losses of Si, Al, Na, K, and Ca in the damaged zone, and loss of Na, Al, and Ca in the fault core. (b) Traverse across the White Rock thrust shows significant depletion of Na, Si, K, and Al in the cataclasite and ultracataclasite core of the fault.

$$+0.3\text{ g }Fe_2O_3 + 0.1\text{ g }K_2O + 0.6\text{ g LOI.} \quad (10)$$

Silica is slightly enriched in the gouge/cataclasite zone relative to the damaged zone, and small amounts of fluid–rock interactions in the damaged zone are suggested by these results.

Immobile components plot well above the isovolume isocon for the White Rock thrust ultracataclasite zone (Fig. 5c). The constant mass isocon has a slope of one, and the constant volume isocon has a slope of 0.95 ($\rho^{fa}_{ultra.}/\rho^{pr} = 2.62/2.75$). The immobile isocon is best-fit through TiO_2, MnO, MgO and P_2O_5, and leads to a slope of 2.77. Using equations (7) and (8), mass loss is approximately 64% and volume loss ranges from 36% to 77%. The balanced component equation for the White Rock fault core is:

100 g protolith granite

$$-50.7\text{ g }SiO_2 - 8.9\text{ g }Al_2O_3 - 0.2\text{ g }Fe_2O_3$$
$$-0.7\text{ g CaO} - 2.8\text{ g }Na_2O - 2.7\text{ g }K_2O$$
$$\rightarrow 31.7\text{ g ultracataclasite} + 0.3\text{ g MgO} + 2.0\text{ g LOI.} \quad (11)$$

Gains or losses of other components were negligible.

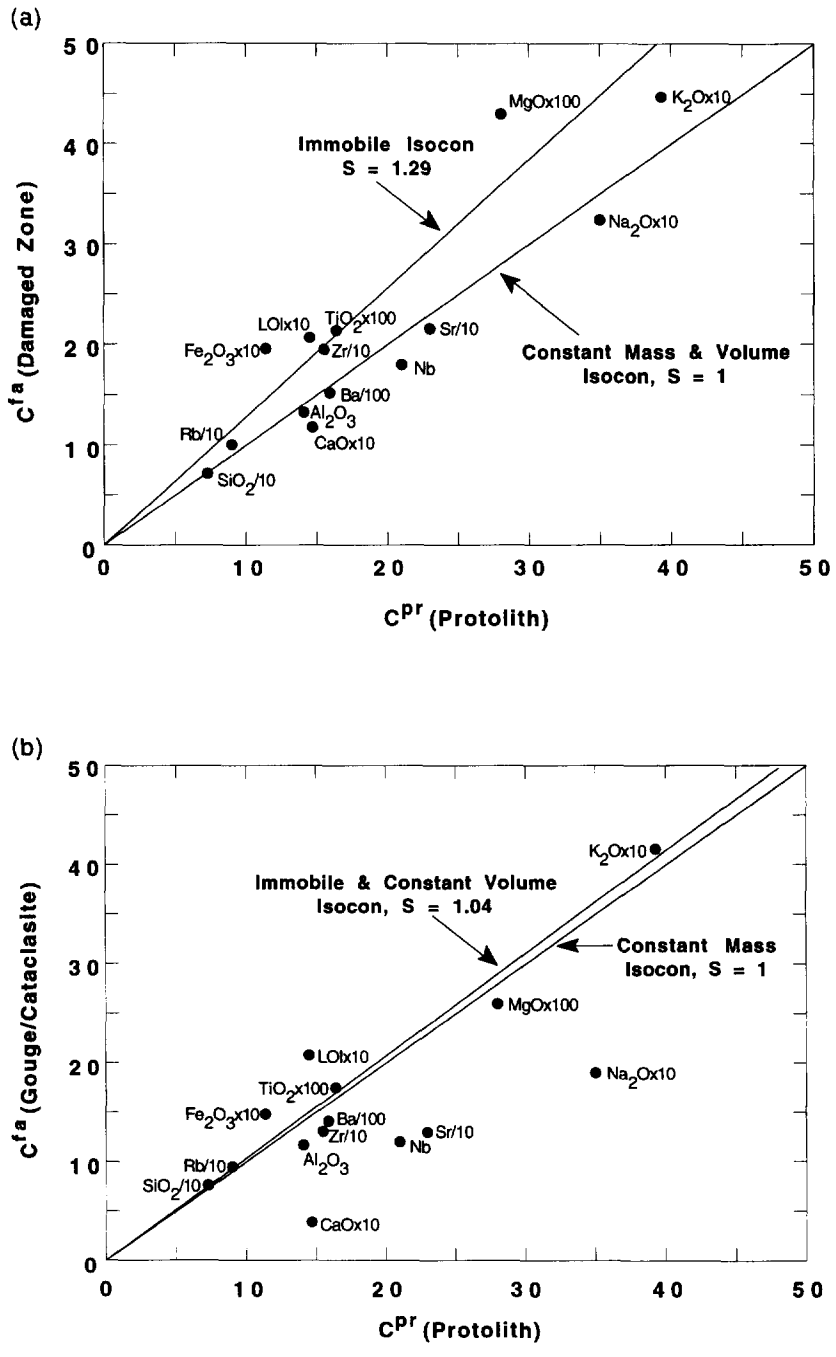

Fig. 5.

The fluid–rock ratios implied by the above reactions can be calculated if the following criteria are known or are assumed: (1) silica loss can be determined (see Gresens 1967, O'Hara 1988), (2) saturation of the fluid with respect to silica, and (3) an estimated temperature of deformation. Fluid–rock weight and volume ratios required to produce the observed silica depletions can thus be calculated. The fluid–rock weight or volume ratio (N) is based on calculated silica losses from the rock. Fluid–rock ratios are only a minimum value for the quantity of water passing through the rock, in that the ratios do not account for fluid that does not chemically interact with rock, nor for fluid that is 100% saturated with respect to silica. The calculations use assumptions regarding the chemistry of the system and imply nothing about the type of flow (single-pass vs reflux).

We calculate the weight and volume of fluid required to produce estimated volume losses on the basis of silica loss from the fault zone. We use silica to calculate fluid–rock ratios because: (1) the evidence for its mobility and the large losses relative to the protolith, and (2) extensive data exists on silica solubility at a range of temperatures and pressures (Walther & Helgeson 1977, Barnes 1979, Rimstidt & Barnes 1980, Fournier & Potter 1982). Using only silica and ignoring the losses of the alkali elements in the calculations underestimates the rock volume transported from the fault zone, and may slightly overestimate the fluid–rock ratios.

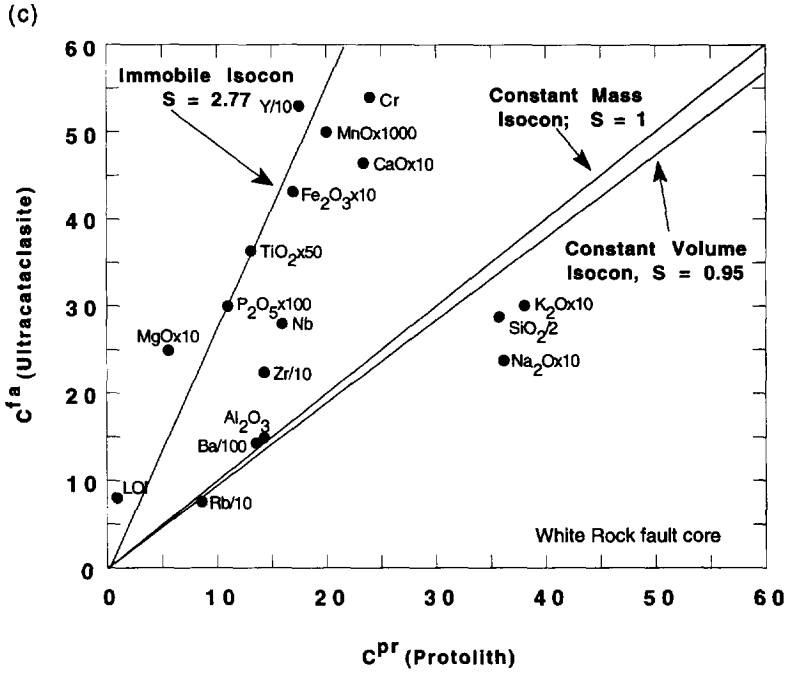

Fig. 5. Grant-type plot of average composition of protolith granite vs average composition of fault core rocks. Concentrations (C) are in wt% (oxides) and ppm (trace elements) scaled to fit on the plot. (a) East Fork fault damaged zone rocks display slight enrichments in immobile elements, with immobile isocon has a slope of 1.29, which is equivalent to a mass and volume loss of 22%. (b) East Fork gouge/cataclasite show virtually no enrichment in immobile elements. The constant volume slope equals the best-fit immobile isocon with a slope of 1.04. This is equivalent to a mass loss of 2.9% (range, 0–3%) and 0% volume loss. (c) Grant-type plot of average composition of protolith granite vs average composition of ultracataclasite for the White Rock fault. Significant enrichments in immobile elements show an immobile isocon with a slope of 2.77, which is equivalent to a mass loss of 64% and a volume loss of 66%. Error within analysis suggests volume loss may range from 36 to 77%. Volume loss in the cataclasite zone is slightly lower (≈50–60%).

Temperature in the White Rock thrust likely ranged from 350°C (at the breach of the Precambrian rocks) to 250°C, and temperatures in the East Fork thrust were <250°C. These temperatures are based on: (1) cross-section restorations (Mitra 1984, Evans 1993), (2) mineral assemblages [e.g. kaolinite and laumontite are not stable at temperatures above 300–350°C (Montoya & Hemley 1975, Hemley *et al.* 1980, Frey 1987)], (3) an assumed geothermal gradient of ~30°C km^{-1}, (4) dominant deformation mechanisms in the White Rock and East Fork faults, and (5) rocks we sampled all come from the hanging wall side of the faults, and thus the rocks were uplifted and cooled from their original depths. Silica solubilities used are based on the data of Fournier & Potter (1982) for silica saturations of 0–90%. Fluid likely encountered silica throughout its path in the fault zone, and therefore silica saturation were probably much closer to 90% during the fault development. We use a range of saturations to provide the widest estimates of the volume of fluid in the fault zone.

Fluid–rock ratios for the East Fork damaged zone and White Rock ultracataclasite zone were calculated using the relationship:

$$\mathbf{N_W} = \mathbf{L_{Si}}/\mathbf{C^f_{Si}}(1 - s), \mathbf{N_V} = \mathbf{N_W}\rho^{pr}, \qquad (12)$$

where $\mathbf{N_W}$ is the fluid–rock weight ratio, $\mathbf{N_V}$ is the volumetric fluid–rock ratio, ρ^{pr} is the density of the protolith, $\mathbf{L_{Si}}$ is the loss of silica in the fault relative to the protolith granite measured in grams of silica lost per 100 grams of rock, $\mathbf{C^f_{Si}}$ is the concentration of silica in the fluid in grams of silica per grams of solute and s is the fractional saturation of the fluid with respect to silica. Values of silica depletion ($\mathbf{L_{Si}}$) used were 18.6 g silica/100 g rock (East Fork damaged zone) and 50.7 g/100 g rock (White Rock ultracataclasite zone), silica solubilities correspond to temperatures from 350 to 150°C, and saturation with respect to silica ranging from 0 to 90%. The estimates of fluid–rock ratios are summarized in Table 2 and in Fig. 6. Due to the nature and number of assumptions inherent in computation of fluid–rock values, the values are probably valid only as order of magnitude estimates. The calculations yield F/R values of 10^2–10^4 (Table 2).

Fluid–rock volume ratios of 10^2–10^4 seem large, but when considered over the life of the faults, these fluid/rock volumes are reasonable. We estimate fluid flux involved in creating the volume losses by fluid transport by assuming: (1) the maximum and minimum life of the faults and ensuing fluid–rock interaction were 20 Ma (Dickinson *et al.* 1988) and 1 Ma, respectively, (2) other parameters stated above, (3) comparable deformation and fluid–rock interaction occurred over a stretch of fault about one kilometer in length and 10 m wide. In this case, water is channeled up a 1 km long, 10 m wide (cross-section view) by 1 m wide (map view) fault conduit (i.e. 10,000 m^3 of fault). The fluid flux (**q**) determines the volume of fluid that passes through a fault conduit in a given period of time (1–20 Ma). For example:

$$[10{,}000\ \text{m}^3 \times (\mathbf{N_V})]/[10\ \text{m}^2\ (\text{conduit}) \times 20\ \text{Ma}]$$

Table 2. Fluid–rock weight and volume ratios as they relate to varying temperatures and silica saturation regimes for the East Fork and White Rock faults. Temp. (°C) is the temperature within the fault zone, Sat. is the saturation of fluid with respect to silica, N_W is the fluid–rock weight ratio, and N_V is the fluid–rock volume ratio

White Rock thrust L_{Si} = 50.7 g/100 g				East Fork fault L_{Si} = 18.6 g/100 g			
Temp. (°C)	Sat.	N_W	N_V	Temp. (°C)	Sat.	N_W	N_V
350	0%	207	569	350	0%	76	201
	40%	345	949		40%	127	335
	70%	690	1900		70%	253	668
	90%	2070	5690		90%	759	2000
300	0%	355	976	300	0%	130	343
	40%	591	1630		40%	216	570
	70%	1180	3250		70%	434	1150
	90%	3550	9750		90%	1300	3440
250	0%	677	1830	250	0%	245	647
	40%	1110	3060		40%	408	1080
	70%	2220	6120		70%	816	2150
	90%	6670	18,300		90%	2450	6460
200	0%	1330	3670	200	0%	489	1290
	40%	2220	6120		40%	816	2150
	70%	4450	12,200		70%	1630	4310
	90%	13,300	36,700		90%	4900	12,900
150	0%	3380	9300	150	0%	1240	3270
	40%	5630	15,500		40%	2070	5460
	70%	11,300	31,000		70%	4130	10,900
	90%	33,800	93,000		90%	12,400	32,700

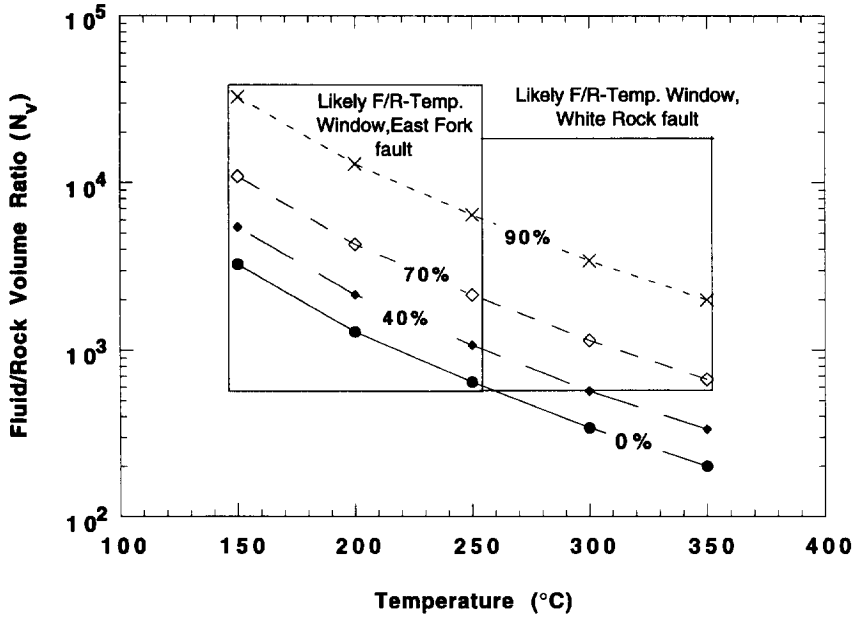

Fig. 6. Inferred fault zone temperature vs fluid–rock volume ratios for the East Fork fault and the White Rock fault, for different values of silica saturation as indicated. Likely F/R-temp window represents the likely fluid–rock volume ratios that may have existed in the fault zone based on fault zone temperature constraints of 150–250°C for the East Fork fault and 250–350°C for the White Rock fault. Ratios for both faults range from $\sim 10^2$–10^4.

$$= \mathbf{q} = 5 \times 10^4 \text{ m Ma}^{-1} \text{ or } 10^{-9} \text{ m s}^{-1}. \quad (13)$$

Calculated fluid fluxes based on the above stated criteria range from 10^{-6} m s^{-1} to 10^{-9} m s^{-1} (Fig. 7) or fluid–rock volume ratios over time of 0.005 L m^{-3} of rock·y and 0.50 L m^{-3} of rock·y. These values of fluid flux are similar to those calculated by Forster & Evans (1991) in a numerical flow model based on a thrust fault of similar character as the East Fork and White Rock thrusts. Thus, the geochemical analyses presented above and the resulting estimates of flux are entirely consistent with topographically-driven, steady-state regional flow in a crystalline thrust sheet.

Both fault zones have similar values of fluid flux. Since fluid flux values are based on volumetric losses of silica from the fault, less fluid flux is required to remove large amounts of material from the 'hotter' White Rock thrust, whereas more fluid flux is required to remove

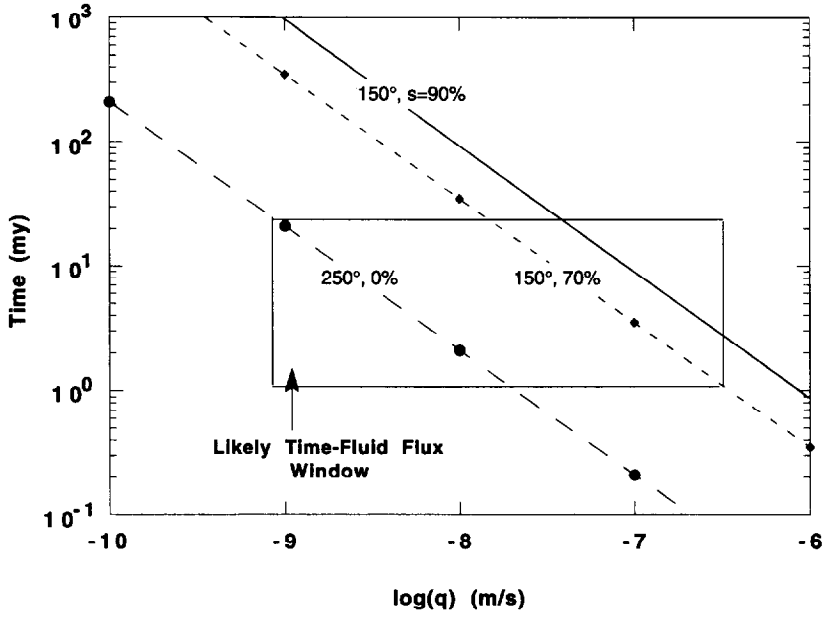

Fig. 7. Fluid flux (q) vs time required to create the estimated volumetric losses within the East Fork fault and the White Rock fault. Likely time–fluid flux window represents the likely fluid flux that may have existed in the fault zone based on the time constraint of between 20 Ma and 1 Ma, fluid saturation with respect to silica between 0 and 90%, and fault zone temperature constraints of 150–250°C for the East Fork fault and 250–350°C for the White Rock fault. Fluid fluxes in the fault zones may have ranged from 10^{-6} m s^{-1} to 10^{-9} m s^{-1}, but were probably closer to the lower end.

small amounts of material from the 'cooler' East Fork fault.

These calculations indicate that large fluid fluxes have caused volume losses in the White Rock thrust by removal of large amounts of mobile components (SiO_2, Al_2O_3, K_2O, Na_2O and CaO) from the system. The large losses of silica and alkalis are consistent with the breakdown of quartz, feldspar and biotite–kaolinite, montmorillonite, and laumontite and the removal of the dissolved cations. Rocks from the East Fork fault do not exhibit the same volume loss for roughly equivalent F/R values, which is consistent with lower temperatures, lower solubilities, and higher saturation expected at the shallower levels.

DISCUSSION AND CONCLUSIONS

We examined the structure, microstructure and geochemistry of the White Rock and East Fork faults to evaluate the role of fluids in the development of the faults. At shallow structural levels, unaltered protolith grades into randomly-fractured, slightly-deformed protolith, which grades into a damaged zone characterized by an increase in micro-scale to outcrop-scale, interconnected, fault-subparallel fractures, increased alteration and mineralization. The fault core consists of interleaved zones of fine-grained gouge and cataclasites, bounded by pods of gouge, breccia, and protocataclasite. Boundaries between protolith and damaged zone are commonly gradational, and the boundaries between damaged zone and fault core are diffuse (Evans 1988).

A mature portion of faults at deeper structural levels (~10–12 km) also exhibits a zonation into protolith, damaged zone, and fault core. The major differences at this level are that the fault core contains an intensely deformed zone of foliated and nonfoliated ultracataclasites, bounded by anastomozing zones of intensely veined protocataclasites and cataclasites, and the boundary between fault core and damaged zone is very sharp.

Geochemical analyses document varying degrees of fluid–rock interaction at different structural levels and in different parts of each fault zones. The White Rock thrust experienced up to 70% volume loss which accompanied deformation, fluid-enhanced alteration, and formation of laumontite veins in the damaged zone. Shallow-level faults of the East Fork fault exhibit little volume loss, limited fluid-assisted syntectonic alteration, and abundant quartz veins. Alteration and fluid–rock interaction measured by the geochemical analyses also increases towards the damaged zone and fault core. Our observations indicate that fluids penetrated the White Rock thrust and were involved in dissolution and transport of Si, Na, and other alkalis, which resulted in rock volume loss during deformation, whereas the East Fork faults experienced little alteration, deposition of quartz veins, and little rock volume loss. Fluid–rock ratios in the fault zones are 10^2–10^4, which yields fluid fluxes of 10^{-6}–10^{-9} m s^{-1}.

We couple our observations with regional scale flow models of crystalline thrust sheets (Forster & Evans 1991), estimates of the permeability of the faults (Goddard 1993, Forster *et al.* 1994), and structural models for the fault zone geometry (Evans 1993, Mitra 1984) to infer that fluids penetrated the thrust sheets to regions adjacent to the fault while they were active. Damaged zone rocks provided enhanced permeability relative to the protolith for the fluids. Topographically driven fluid flow could occur up-dip in the fault zones and would

result in transport of soluble cations either locally or over significant portions of the fault. Deeper levels of the faults, as suggested by the White Rock thrust data, experience greater fluid–rock interaction and volume loss. Flow of fluids to shallower levels would have decreased pressure and temperatures, reducing the solubility of the silica (Fournier & Potter 1982) and resulted in the deposition of quartz. As fault slip increases, the fault core evolves from the damaged zone, and dissolution of soluble elements increases. The fine-grained alteration, comminution, and diffusive mass transfer products in the fault core may result in a zone of extremely low, and anisotropic permeability (Forster *et al.* 1994).

Petrologic, geochemical and isotopic studies indicate large fluid-related rock volume loss (>70%) may occur, and fluid–rock ratios of 10^1–10^4 record large fluid fluxes that circulated through fault and shear zones (Engelder 1984, Kerrich 1986, O'Hara 1988, Sinha *et al.* 1988, Losh 1989, O'Hara & Blackburn 1989, Glazner & Bartley 1991, Selverstone *et al.* 1991). Our results yield similar values for fluid–rock ratios and volume losses for faults which developed in the brittle-plastic and brittle regimes. These results indicate the style and degree of fluid rock interaction in faults in the upper part of the crust may vary with depth and with the intensity of deformation. The fractured and faulted damaged zone adjacent to the fault core may exhibit greater fluid–rock chemical and mechanical interactions, and may be the zone by which fluids are supplied to the fault zone. The results here support earlier microstructural work on these faults that deformation and fluid flow were tightly linked in both of these faults (Mitra 1984, 1990, Evans 1988, 1990).

Acknowledgements—This work was supported by NSF grant (EAR 90-05027) to Evans and C. B. Forster and Goddard was also supported by a Seely-Hinckley Fellowship from the Graduate College at Utah State University. Assistance in the field and laboratory from C. M. Brown, K. Davis and D. Hinton is gratefully acknowledged. Reviews by K. O'Hara and S. Reynolds improved the paper, and discussions with R. Bruhn, J. S. Caine, C. B. Forster and W. T. Parry helped in our understanding fluid–rock interactions.

REFERENCES

Barnes, H. L. 1979. *Geochemistry of Hydrothermal Ore Deposits*. John Wiley & Sons, New York.

Brantley, S. L., Evans, B., Hickman, S. H. & Crerar, D. A. 1990. Healing of microcracks in quartz: implications for fluid flow. *Geology* **18**, 136–139.

Bruhn, R. L., Yonkee, W. A. & Parry, W. T. 1990. Structural and fluid–chemical properties of seismogenic normal faults. *Tectonophysics* **175**, 139–157.

Chester, F. M., Evans, J. P. & Biegel, R. L. 1993. Internal structure and weakening mechanisms of the San Andreas Fault. *J. geophys. Res.* **98**, 771–786.

Chester, F. M. & Logan, J. M. 1986. Implications for mechanical properties of brittle faults from observations of the Punchbowl fault zone, California. *Pure & Appl. Geophys.* **124**, 80–106.

Correns, C. W. 1978. Titanium: behavior in metamorphic reactions. In: *Handbook of Geochemistry* (edited by Wedepohl, K. H.). Springer, Berlin.

Dickinson, W. R., Klute, M. A., Hayes, M. J., Janecke, S. U., Lundin, E. R., McKittrick, M. A. & Olivares, M. D. 1988. Paleogeographic and paleotectonic setting of Laramide sedimentary basins in the central Rocky Mountain region. *Bull. geol. Soc. Am.* **100**, 1023–1039.

Dostal, J., Strong, D. F. & Jamieson, R. A. 1980. Trace element mobility in the mylonite zone within the ophiolite aureole, St. Anthony complex, Newfoundland. *Earth & Planet Sci. Lett.* **49**, 188–192.

Engelder, T. 1984. The role of pore water circulation during the deformation of foreland fold and thrust belts. *J. geophys. Res.* **89**, 4319–4325.

Evans, J. P. 1988. Deformation mechanisms in granitic rocks at shallow crustal levels. *J. Struct. Geol.* **10**, 437–443.

Evans, J. P. 1990. Textures, deformation mechanisms, and the role of fluids in the cataclastic deformation of granitic rocks. In: *Deformation Mechanisms, Rheology and Tectonics* (edited by Knipe, R. J. & Rutter, E. H.). *Spec. Pub. geol. Soc. Lond.* **54**, 29–39.

Evans, J. P. 1993. Deformation mechanisms and kinematics of a crystalline thrust sheet: the Washakie thrust system, Wyoming. In: *Basement Deformation in Rocky Mountain Foreland Structures* (edited by Schmidt, C. J., Chase, R. & Erslev, E. A.). *Spec. Pap. geol. Soc. Am.* **280**, 147–161.

Faure, G. 1991. *Principles and Applications of Inorganic Geochemistry*. Macmillan Publishing Company, New York.

Floyd, P. A. & Winchester, J. A. 1983. Element mobility associated with meta-shear zones within the Ben Hope amphibolite suite, Scotland. *Chem. Geol.* **39**, 1–15.

Forster, C. B. & Evans, J. P. 1991. Hydrogeology of thrust faults and crystalline thrust sheets: results of combined field and modeling studies. *Geophys. Res. Lett.* **18**, 979–982.

Forster, C. B., Goddard, J. V. & Evans, J. P. 1994. Permeability structure of a thrust fault. In: *U.S. Geological Survey Open-file report, Fluids and Faulting* (edited by Bruhn, R. L., Hickman, S. & Sibson, S.).

Fournier, R. O. & Potter, R. W. 1982. An equation correlating the solubility of quartz in water from 25°C to 900°C at pressures up to 10,000 bars. *Geochim. cosmochim. Acta* **46**, 1969–1973.

Frey, M. 1987. *Low Temperature Metamorphism*. Blackie & Son Limited, Glasgow.

Garrels, R. M. & Christ, C. L. 1965. *Solutions, Mineral and Equilibria*. Freeman, Cooper & Company, 352–370.

Glazner, A. F. & Bartley, J. M. 1991. Volume loss, fluid flow and state of strain in extensional mylonites from the central Mojave Desert, California. *J. Struct. Geol.* **13**, 587–594.

Goddard, J. V. 1993. Internal deformation, evolution and fluid flow in basement-involved thrust faults, northwest Wyoming. M.Sc. thesis, Utah State University, Logan.

Grant, J. A. 1986. The isocon diagram—a simple solution to Gresens' equation for metasomatic alteration. *Econ. Geol.* **81**, 1976–1982.

Gresens, R. L. 1967. Composition–volume relationships of metasomatism. *Chem. Geol.* **2**, 47–65.

Hanson, G. N. 1980. Rare earth elements in petrogenetic studies of igneous systems. *Ann. Rev. Earth & Planet Sci.* **8**, 371–406.

Hemley, J. J., Montoya, J. W., Marinenko, J. W. & Luce, R. W. 1980. Equilibria in the system Al_2O_3–SiO_2–H_2O and some general implications for alteration/mineralization processes. *Econ. Geol.* **75**, 210–228.

Hickman, S. H. 1991. Stress in the lithosphere and the strength of active faults. *U.S. Nat. Rep. to Internat. Un. of Geodesy and Geophys.* 1987–1990, *Reviews of Geophys., Suppl.* 759–775.

Janecke, S. U. & Evans, J. P. 1988. Feldspar-influenced rock rheologies. Geology **16**, 1064–1067.

Kerrich, R. 1986. Fluid infiltration into fault zones: Chemical, isotopic and mechanical effects. *Pure & Appl. Geophys.* **124**, 225–268.

Losh, S. 1989. Fluid–rock interaction in an evolving ductile shear zone and across the brittle–ductile transition, central Pyrenees, France. *Am. J. Sci.* **289**, 600–648.

McCaig, A. M. 1988. Deep fluid circulation in fault zones. *Geology* **16**, 867–870.

Mitra, G. 1984. Brittle to ductile transition due to large strains along the White Rock thrust, Wind River Mountains, Wyoming. *J. Struct. Geol.* **6**, 51–61.

Mitra, G. 1990. Deformation of granitic basement rocks along fault zones at shallow to intermediate crustal levels. In: *Structural Geology of Fold and Thrust Belts* (edited by Mitra, S. & Fisher, G). Johns Hopkins Press, 123–144.

Mitra, G. & Frost, R. B. 1981. Mechanisms of deformation within Laramide and Precambrian deformation zones in basement rocks of the Wind River Mountains. *Contr. Geol.* **19**, 161–173.

Mitra, G., Hull, J. M., Yonkee, W. A. & Protzman, G. M. 1988. Comparison of macroscopic and microscopic deformational styles in

the Idaho–Wyoming thrust belt and the Rocky Mountain foreland. *Mem. Geol. Soc. Am.* **171**, 119–130.

Montoya, J. W. & Hemley, J. J. 1975. Activity relations and stabilities in alkali feldspar and mica alteration reactions. *Econ. Geol.* **70**, 577–583.

Moore, J. C. 1989. Tectonics and hydrogeology of accretionary prisms. *J. Struct. Geol.* **11**, 95–106.

O'Hara, K. 1988. Fluid flow and volume loss during mylonitization: an origin for phyllonite in an overthrust setting, North Carolina, U.S.A. *Tectonophysics* **156**, 21–36.

O'Hara, K. & Blackburn, W. H. 1989. Volume loss model for trace-element enrichment in mylonites. *Geology* **17**, 524–527.

Parry, W. T. & Bruhn, R. L. 1990. Fluid pressure transients on seismogenic normal faults. *Tectonophysics* **179**, 335–344.

Reynolds, S. J. & Lister, G. S. 1987. Structural aspects of fluid–rock interactions in detachment zones. *Geology* **15**, 362–366.

Richmond, G. M. 1945. Geology of northwestern end of the Wind River Mountains, Sublette County, Wyoming. U.S.G.S. Oil & Gas Inv. Map 31.

Rimstidt, J. D. & Barnes, H. L. 1980. The kinetics of silica–water reactions. *Geochim. cosmochim. Acta* **44**, 1683–1699.

Selverstone, J., Morteani, G. & Staude, J. M. 1991. Fluid channelling during ductile shearing: transformation of granodiorite into aluminous schist in the Tauren Window, eastern Alps. *J. Metamor. Geol.* **9**, 419–431.

Sibson, R. H. 1981. Fluid-flow accompanying faulting: field evidence and models. In: *Earthquake Prediction* (edited by Simpson, D. W. & Richards, P. G.). *Am. Geophys. Un., Ewing Series Mono* 593–603.

Sibson, R. H. 1987. Earthquake rupturing as a mineralizing agent in hydrothermal systems. *Geology* **15**, 701–704.

Sibson, R. H., Robert, F. & Poulsen, K. H. 1988. High-angle reverse faults, fluid pressure cycling and mesothermal gold–quartz deposits. *Geology* **16**, 551–555.

Sinha, A. K., Hewitt, D. A. & Rimstidt, J. D. 1986. Fluid interaction and element mobility in the development of ultramylonites. *Geology* **14**, 833–886.

Sinha, A. K., Hewitt, D. A. & Rimstidt, J. D. 1988. Metamorphic petrology and strontium isotope geochemistry associated with development of mylonites: an example from the Brevard fault zone, North Carolina. *Am. J. Sci.* **288**, 115–147.

Thompson, A. B. 1971. P CO_2 in low-grade metamorphism; zeolite, carbonate, clay mineral, prehnite relations in the system CaO–Al_2O_3–SiO_2–CO_2–H_2O. *Contrib. Mineral. Petrol.* **33**, 145–161.

Vocke, R. D., Hanson, G. N. & Grunenfelder, M. 1987. Rare Earth element mobility in the Roffna Gneiss. *Contrib. Mineral Petrol.* **95**, 145–154.

Walther, J. V. & Helgeson, H. C. 1977. Calculation of the thermodynamic properties of aqueous silica and the solubility of quartz and its polymorphs at high pressures and temperatures. *Am. J. Sci.* **277**, 1315–1351.

Winchester, J. A. & Max, M. D. 1984. Element mobility associated with syn-metamorphic shear zones near Scotchport, NW Mayo, Ireland. *J. Metamor. Geol.* **2**, 1–11.

Yonkee, W. A. & Mitra, G. 1993. Comparison of basement deformation styles in parts of the Rocky Mountain Foreland, Wyoming, and the Sevier orogenic belt, northern Utah. In: *Basement Deformation in Rocky Mountain Foreland Structures* (edited by Schmidt, C. J., Chase, R. & Erslev, E. A.). *Spec. Pap. geol. Soc. Am.* **280**, 197–228.

Zen, E-An. 1961. The zeolite facies: an interpretation. *Am. J. Sci.* **259**, 401–409.